Quantum squeezing via self-induced transparency in a photonic crystal fiber

M. S. Najafabadi [1,*] L. L. Sánchez-Soto [1,2] J. F. Corney [3] N. Kalinin [1,4] A. A. Sorokin [5] and G. Leuchs [1,4]

[1]*Max-Planck-Institut für die Physik des Lichts, 91058 Erlangen, Germany*

[2]*Departamento de Óptica, Facultad de Física, Universidad Complutense, 28040 Madrid, Spain*

[3]*School of Mathematics and Physics, University of Queensland, Brisbane, Queensland 4072, Australia*

[4]*Institut für Optik, Information und Photonik, Friedrich-Alexander-Universität Erlangen-Nürnberg, 91058 Erlangen, Germany*

[5]*A. V. Gaponov-Grekhov Institute of Applied Physics of the Russian Academy of Sciences, 46 Ulyanov Street, 603950 Nizhny Novgorod, Russia*

(Received 30 October 2023; accepted 17 April 2024; published 8 May 2024)

We study the quantum squeezing produced in self-induced transparency in a photonic crystal fiber by performing a fully quantum simulation based on the positive P representation. The amplitude squeezing depends on the area of the initial pulse: When the area is 2π, there is no energy absorption and no amplitude squeezing. However, when the area is between 2π and 3π, one observes amplitude-dependent energy absorption and a significant amount of squeezing. We also investigate the effect of damping, detuning, and temperature: The results indicate that a heightened atom-pulse coupling, caused by an increase in the spontaneous emission ratio, reduces the amplitude squeezing.

DOI: 10.1103/PhysRevResearch.6.023142

I. INTRODUCTION

Self-induced transparency (SIT) in two-level atomic systems is one of the most well-known coherent pulse propagation phenomena: Above a certain intensity threshold, the absorption of a pulse by resonant transitions decreases strongly and the medium becomes almost completely transparent, which is accompanied by a considerable reduction in the group velocity (for reviews, see Refs. [1–4]). This was first reported by McCall and Hahn [5,6], who, by using a semiclassical description, demonstrated that the two-level medium becomes transparent to a 2π pulse through a strong absorption. This semiclassical model is nowadays standard in quantum-optics textbooks that study the effects of atomic coherence [7–9].

The SIT solitons have been proposed as candidates for pulsed squeezed-state generation [10], quantum nondemolition measurements [11], and quantum information storage and retrieval [12]. Moreover, with the recent advances in microstructured fiber technologies [13], the generation of squeezing via SIT solitons inside gas-filled single-mode photonic crystal fibers is being considered [14], which simplifies transverse effects.

In all these advances, the quantum noise and the quantum correlations play a dominant role that cannot be captured by any semiclassical approach. Therefore, a full quantum approach to SIT is an essential step toward a complete understanding of the physics involved. A theory of SIT using a linearization ansatz has been developed [15] within the framework of the inverse-scattering method [16]. A further refinement was suggested by using a coarse-grain-averaged light-atom interaction [17] and treating the quantum noise by the backpropagation method [18], which can take into account the field continuum contributions and the atomic fluctuations generally.

These results, important as they are, do not provide proper guidelines for realistic experiments, because they fail to account for any limitations on the squeezing. In this paper, we take an alternative route and adapt a method to deal with the propagation of radiation in an optically pumped two-level medium that has collisional and radiative damping [19]. The idea is to derive a set of stochastic c-number differential equations that are equivalent to the Heisenberg operator equations. This is accomplished through use of the positive P representation [20], which provides a probabilistic description in which stochastic averages correspond to normally ordered correlations. The method has the advantage of yielding equations that may be solved numerically, while keeping the key elements that characterize the quantum nature of the field.

On the experimental side, when sending a light pulse through an atomic ensemble, the response of each atom will depend on the field amplitude at its respective position, leading to a transverse structure in the resulting light field and in the atomic ensemble as well. This situation changes if the atoms interact with only one single mode of the field. Then, each photon interacts with all atoms and no transverse structure will develop. To achieve this situation, one might think, e.g., of a glass capillary as a waveguide, but this would not be a good waveguide as it is lossy by coupling to modes

*mojdeh.shikhali-najafabadi@mpl.mpg.de

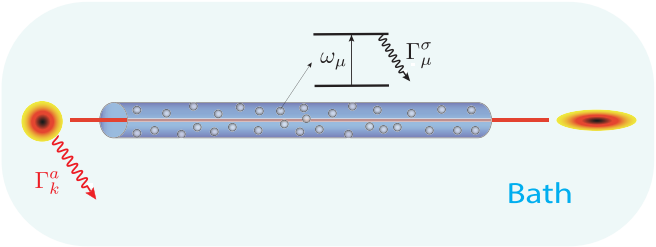

FIG. 1. Schematics of the propagation of a coherent pulse in a medium consisting of N two-level atoms in a hollow-core fiber. The system (including both the coherent field and the atoms) interacts with the bath, but the interaction between the atoms is considered negligible.

propagating to the sides out of the capillary. Lossless guiding by total internal reflection requires a higher index in the core, which is not possible with a simple capillary. But a photonic crystal fiber (PCF) [13] provides both nearly lossless guiding and a hollow core for the atom vapor. An additional advantage of a PCF is that the decay of the atoms in the core into modes other than the single longitudinal mode is largely suppressed.

The plan of this paper is as follows. In Sec. II we introduce the model Hamiltonian, investigating how the quantum noise sources arise as coming from both damping and nonlinearities in the Hamiltonian. We explore the dynamics by numerically solving the fully nonlinear stochastic differential equations emerging from the positive P representation. The additional effect of damping, reservoir noise, and atom-field coupling is also investigated. In Sec. III we present the main results of our model. We show that the pulse area indeed is the crucial quantity in observing the amplitude squeezing for SIT solitons. Due to the complexity of the dynamics in the expanded phase space, one needs a high number of samples to increase the accuracy of the method. We discuss the effect of pulse reshaping on the squeezing, as well as the role of damping and temperature. Our results indicate that the stronger the atom-field coupling, the less is the amplitude squeezing. Finally, our concluding remarks are presented in Sec. IV.

II. MODEL

A. Hamiltonian

Following the ideas of Ref. [19], we first introduce a suitable Hamiltonian that describes the interaction of an ensemble of two-level atoms with a single mode of the radiation field. A schematic picture of our model is shown in Fig. 1. In the rotating-wave and dipole approximations the model Hamiltonian reads as

$$\hat{H} = \hat{H}_{\rm A} + \hat{H}_{\rm F} + \hat{H}_{\rm B} + \hat{H}_{\rm FB} + \hat{H}_{\rm AB} + \hat{H}_{\rm AF}, \tag{2.1}$$

where

$$\hat{H}_{\rm A} = \frac{1}{2}\sum_\mu \hbar\omega_\mu \hat{\sigma}^3_\mu,$$

$$\hat{H}_{\rm F} = \sum_k \hbar\omega_k\, \hat{a}^\dagger_k \hat{a}_k,$$

$$\hat{H}_{\rm B} = \hat{H}^a + \hat{H}^\sigma + \hat{H}^z,$$

$$\hat{H}_{\rm AF} = \hbar\sum_k\sum_\mu \left(g\hat{a}^\dagger_k \hat{\sigma}^-_\mu e^{-ikz_\mu} + {\rm H.c.}\right),$$

$$\hat{H}_{\rm AB} = \hbar\sum_\mu \left(\hat{\Gamma}^{\sigma^\dagger}_\mu \hat{\sigma}^-_\mu + \hat{\Gamma}^\sigma_\mu \hat{\sigma}^+_\mu + \hat{\Gamma}^3_\mu \hat{\sigma}^3_\mu\right),$$

$$\hat{H}_{\rm FB} = \hbar\sum_k \left(\hat{\Gamma}^{a^\dagger}_k \hat{a}_k + \hat{\Gamma}^a_k \hat{a}^\dagger_k\right). \tag{2.2}$$

Here, $\hat{H}_{\rm A}$ is the free Hamiltonian of the atoms, with ω_μ the resonant frequency of the μth atom described in terms of the standard Pauli operators [21], and $\hat{H}_{\rm F}$ is the free Hamiltonian of the paraxial field modes propagating in the fiber, each one having frequency ω_k and with an annihilation operator $\hat{a}_k$ (for a single polarization).

The piece $\hat{H}_{\rm B}$ is the free Hamiltonian of the baths corresponding to field modes $\hat{H}^a$, atomic dipoles $\hat{H}^\sigma$, and collisions $\hat{H}^z$. In addition, $\hat{H}_{\rm AF}$ is the interaction of the paraxial field with dipole-field coupling g; $\hat{H}_{\rm AB}$ is the interaction of atomic and collisional reservoirs with atoms and, finally, $\hat{H}_{\rm FB}$ is the interaction of the background reservoir with the radiation field.

Let us briefly discuss the physics behind the bath terms in (2.1). The paraxial modes are coupled to a background of absorbing dipoles $\hat{\Gamma}^a_k$, with free Hamiltonian $\hat{H}^a$. This describes background absorption and reemission due to other atoms in the medium, as opposed to the resonant ones.

In general, the atoms are also coupled to modes with nonparaxial wave vectors, which form independent radiative reservoirs for each atom, whose operators are $\hat{\Gamma}^\sigma_\mu$. The free Hamiltonian of these atomic reservoirs is $\hat{H}^\sigma$. This approximation of independent reservoirs neglects any transverse dipole-dipole coupling and is thus valid only for relatively low-density optical media, where local-field corrections are negligible. Any optical pumping is also included in these reservoirs.

Finally, the operators $\hat{\Gamma}^3_\mu$describe a coupling of the resonant atoms to a collisional phase-damping reservoir with free Hamiltonian $\hat{H}^z$, which describes weak collisions with nonresonant atoms.

To enable a continuous description, we first divide the available volume up into small elements of size ΔV centered at positions $\mathbf{r}_j$ along the fiber and containing N_j resonant atoms. The density of resonant atoms in a certain position $\mathbf{r}$ and a certain frequency ω can then be defined as

$$\rho(\mathbf{r}_j, \omega) = \frac{N_j}{\Delta V} f_\omega(\omega), \tag{2.3}$$

where $f(\omega)$ is a spectral line shape [22]. The medium can be considered to be either homogeneously (i.e., Lorentz) or inhomogeneously (i.e., Gaussian) broadened around a central frequency ω_0.

The dipole-field coupling is assumed to be identical for all the atoms and independent of the frequency and the wave vector. For an ideal two-level atom this coupling reads [7]

$$g^2 = \left(\frac{\omega_0 |\mathbf{d}_{12}\cdot\mathbf{e}|^2}{2\hbar\varepsilon_0 V}\right), \tag{2.4}$$

where ω_0 is the resonant frequency, V the quantization mode volume, $\mathbf{d}_{12}$ is the relevant dipole matrix element and $\mathbf{e}$ is the mode polarization.

The evolution of the system can be studied by the master equation for the atom-field system by tracing out the reservoir variables and applying the standard Markov approximation [21],

$$\frac{d\hat{\varrho}}{dt} = \frac{1}{i\hbar}[\hat{H}, \hat{\varrho}] + \hat{\mathcal{L}}_{\rm AB}[\hat{\varrho}] + \hat{\mathcal{L}}_{\rm FB}[\hat{\varrho}], \tag{2.5}$$

where $\hat{\varrho}$ is the density matrix of the system. The Lindbladian superoperators $\hat{\mathcal{L}}_{\rm AB}$ and $\hat{\mathcal{L}}_{\rm FB}$ describe relaxation into the reservoir modes in both atomic and field variables and take the form [23]

$$\begin{aligned}
\hat{\mathcal{L}}_{\rm AB}[\hat{\varrho}] &= \sum_{\mu} \frac{1}{2} W_{21}([\hat{\sigma}_\mu^- \hat{\varrho}, \hat{\sigma}_\mu^+] + [\hat{\sigma}_\mu^-, \hat{\varrho}\sigma_\mu^+]) \\
&\quad + \frac{1}{2} W_{12}([\sigma_\mu^+ \hat{\varrho}, \hat{\sigma}_\mu^-] + [\sigma_\mu^+, \hat{\varrho}\hat{\sigma}_\mu^-]) \\
&\quad + \frac{1}{4}\gamma_p\big([\hat{\sigma}_\mu^3, \hat{\varrho}\hat{\sigma}_\mu^3] + [\hat{\sigma}_\mu^3\hat{\varrho}, \hat{\sigma}_\mu^3]\big), \\
\hat{\mathcal{L}}_{\rm FB}[\hat{\varrho}] &= \frac{1}{2} c\kappa \sum_k (1+\bar{n})([\hat{a}_k\hat{\varrho}, \hat{a}_k^\dagger] + [\hat{a}_k, \hat{\varrho}\hat{a}_k^\dagger]) \\
&\quad + \bar{n}([\hat{a}_k^\dagger\hat{\varrho}, \hat{a}_k] + [\hat{a}_k^\dagger, \hat{\varrho}\hat{a}_k]).
\end{aligned} \tag{2.6}$$

Here, W_{21} is the relaxation rate from the excited to the ground state, W_{12} is the incoherent pumping rate, and $\gamma_p = 3\gamma_0$ is the pure dephasing rate. For the field, κ is the absorption rate during the propagation within the medium and

$$\bar{n} = \frac{1}{\exp\left(\frac{\hbar\omega_0}{k_B T_f}\right) - 1} \tag{2.7}$$

is the mean equilibrium photon number in each reservoir mode of interest with T_f to be the temperature of the field background reservoir. Note that for a PCF, $\bar{n}$ will be the closer to zero the lower are the losses. In that sense $\bar{n}$, albeit not a material property, is determined by the quality of the PCF.

If we consider the thermal temperature of the radiative reservoir for the atoms to be T_a, then

$$W_{21} = \gamma_0(1+\bar{n}_a), \quad W_{12} = \gamma_0\bar{n}_a, \tag{2.8}$$

with the photon occupation number $\bar{n}_a$ given by (2.7) with temperature T_a.

It is customary to define the longitudinal and transverse damping rates as

$$\gamma_\parallel = W_{12} + W_{21}, \quad \gamma_\perp = \gamma_p + \tfrac{1}{2}\gamma_\parallel. \tag{2.9}$$

These coefficients $\gamma_\parallel$ and $\gamma_\perp$ correspond to two different damping mechanisms, namely, longitudinal (population decay) and transverse (dephasing). In the case of population decay, the excited atoms have a spontaneous tendency to decay to the ground state. Since this is a stochastic process, it randomly breaks the coherence of the light field. Consequently, a spontaneous emission decay would constantly interrupt the Rabi oscillations. On the other hand, the transverse damping process causes the excited atoms to undergo an elastic or near-elastic collision, which breaks the phase of the light pulse without modifying the population of the excited state. Eventually, the effect of randomizing the phase of the light field will destroy the Rabi oscillations.

B. Quantum evolution in the slowly varying envelope approximation

We will assume that only one transverse mode of the optical waveguide is relevant (i.e., other transverse modes are either not supported by the waveguide or else are not excited during propagation) and that the transverse mode profile $u(\mathbf{r}_\perp)$ is uniform along the length of the fiber. The relevant electromagnetic modes are those with the wave vector aligned with the waveguide axis (which we take as the z axis), and thus we can define an optical field (scaled to be a Rabi frequency) at position z_l as

$$\hat{\Omega}(z_l) \equiv 2ig\sum_m e^{ik_m z_l}\hat{a}_m, \tag{2.10}$$

where $\hat{a}_m$ are the annihilation operators for modes with frequency ω_m and corresponding wave numbers $k_m = m\Delta k$, where $\Delta k = 2\pi/L$ and L is the quantization length (i.e., length of the fiber). We use the index l to refer to grid positions along the z axis. We further subdivide in transverse directions to create cells centered at locations $\mathbf{r}_j$, each of volume $\Delta V = \Delta A\,\Delta z$, where ΔA is the cells' transverse area. The index for the volume cells j thus includes l for the z grid, together with other indices for the transverse locations.

We define atomic field operators by adding together operators for individual atoms in a given spatial cell at $\mathbf{r}_j$ and within the frequency band centered at ω_m,

$$\begin{aligned}
\hat{R}^3(\mathbf{r}_j, \omega_m) &\equiv \frac{1}{N_{jm}}\sum_n^{N_{jm}} \hat{\sigma}_{jmn}^3, \\
\hat{R}^\pm(\mathbf{r}_j, \omega_m) &\equiv \frac{2}{N_{jm}}\sum_n^{N_{jm}} \hat{\sigma}_{jmn}^\pm,
\end{aligned} \tag{2.11}$$

where the atomic index $\mu = (j, m, n)$ has been expanded so that we can sum over only those atoms satisfying the above conditions. Note that the number of atoms in each spatiofrequency cell can be written as $N_{jm} = \rho(\mathbf{r}_j, \omega_m)\Delta V\,\Delta\omega$, where the density $\rho(\mathbf{r}_j, \omega_m)$ is given in Eq. (2.3).

It can be helpful to consider the Heisenberg equations of motion for these field operators, in the absence of reservoir couplings. We start with the original field modes and individual atomic operators,

$$\begin{aligned}
\frac{d}{dt}\hat{a}_m &= -i\omega_m\hat{a}_m - ig\sum_\mu \hat{\sigma}_\mu^- u^*(\mathbf{r}_{\perp\mu})e^{-ik_m z_\mu}, \\
\frac{d}{dt}\hat{\sigma}_\mu^- &= -i\omega_\mu\hat{\sigma}_\mu^- + ig\hat{\sigma}_\mu^3 u(\mathbf{r}_{\perp\mu})\sum_m \hat{a}_m e^{ik_m z_\mu}, \\
\frac{d}{dt}\hat{\sigma}_\mu^3 &= 2ig\sum_m [\hat{a}_m^\dagger\hat{\sigma}_\mu^- u^*(\mathbf{r}_{\perp\mu})e^{-ik_m z_\mu} - \hat{a}_m\hat{\sigma}_\mu^+ u(\mathbf{r}_{\perp\mu})e^{ik_m z_\mu}],
\end{aligned} \tag{2.12}$$

which can be immediately obtained via the standard commutation relations.

Now, we can use these expressions to calculate the time derivatives of the field operators defined above. For the optical

field,

$$\frac{\partial}{\partial t}\hat{\Omega}(z_l) \simeq -i\sum_{l'}\omega(z_l, z_{l'})\,\hat{\Omega}(z_{l'}) + G\sum_{j|l,m}\Delta A\Delta\omega\rho(\mathbf{r}_j,\omega_m)u^*(\mathbf{r}_{\perp j})\hat{R}^-(\mathbf{r}_j,\omega_m), \tag{2.13}$$

where $G = g^2L$ and the function

$$\omega(z_l, z_{l'}) \equiv \frac{1}{M}\sum_m \omega_m e^{ik_m(z_l - z_l')}, \tag{2.14}$$

with M the number of z bins, describes the dispersive properties of the waveguide. Here, the notation $j|l$ indicates that the sum is over all volume elements located at z_l. Taking the continuum limit, we obtain

$$\frac{\partial}{\partial t}\hat{\Omega}(t,z) = \left(-i\omega_0 - c\frac{\partial}{\partial z}\right)\hat{\Omega}(t,z) + G\int \rho(\mathbf{r},\omega)u^*(\mathbf{r}_\perp)\hat{R}^-(\mathbf{r},\omega)\,d^2\mathbf{r}_\perp d\omega, \tag{2.15}$$

where we have used a first-order Taylor expansion in the dispersive term to account for group velocity, ignoring higher-order dispersive effects.

For the atomic fields, the equations of motion are a little more straightforward,

$$\begin{aligned}\frac{d}{dt}\hat{R}^-(\mathbf{r}_j,\omega_m) &\simeq -i\omega_m\hat{R}^-(\mathbf{r}_j,\omega_m) + u(\mathbf{r}_{\perp j})\hat{\Omega}(z_l)\hat{R}^3(t,\mathbf{r}_j,\omega_m),\\ \frac{d}{dt}\hat{R}^3(\mathbf{r}_j,\omega_m) &= -\frac{1}{2}[u(\mathbf{r}_{\perp j})\hat{\Omega}(z_l)\hat{R}^+(t,\mathbf{r}_j,\omega_m) - u^*(\mathbf{r}_{\perp j})\hat{\Omega}^\dagger(z_l)\hat{R}^-(t,\mathbf{r}_j,\omega_m)],\end{aligned} \tag{2.16}$$

where we have assumed that the frequency band is sufficiently small so that all atoms within the mth band have the same resonance frequency ω_m. The continuum limit is then

$$\begin{aligned}\frac{\partial}{\partial t}\hat{R}^-(t,\mathbf{r},\omega) &= -i\omega\hat{R}^-(t,\mathbf{r},\omega) + u(\mathbf{r}_\perp)\hat{\Omega}(t,z)\hat{R}^3(t,\mathbf{r},\omega),\\ \frac{\partial}{\partial t}\hat{R}^3(t,\mathbf{r},\omega) &= -\frac{1}{2}\big[u(\mathbf{r}_\perp)\hat{\Omega}(t,z)\hat{R}^+(t,\mathbf{r},\omega) - u^*(\mathbf{r}_\perp)\hat{\Omega}^\dagger(t,z)\hat{R}^-(t,\mathbf{r},\omega)\big].\end{aligned} \tag{2.17}$$

The optical and atomic fields can be furthermore transformed to a rotating frame, with the fast optical frequency ω_0 removed, leading to equations for the slowly varying envelopes. This will be used in the next section.

C. Dynamics of the positive *P* distribution

Let us now include the coupling with the reservoirs, but keeping the same approximations as in the previous sections that lead to an effective one-dimensional dynamics. Since a direct numerical simulation of the master equation for an N two-level atom system is extremely difficult, our strategy is to derive the suitable equations of motion in phase space. As heralded in the Introduction, we use the positive P approach [20], which is a normally ordered operator representation such that it identifies the moments of $\hat{\varrho}$ with the corresponding c-number moments of a positive P distribution.

In this approach, we have a mapping $\hat{\Omega} \leftrightarrow \Omega$, $\hat{\Omega}^\dagger \leftrightarrow \Omega^\dagger$, $\hat{R}^\pm \leftrightarrow R^\pm$, $\hat{R}^3 \leftrightarrow R^3$, and, following the standard procedures, the master equation can then be transformed into an equivalent Fokker-Planck equation for $P(\Omega, \Omega^\dagger, R^-, R^+, R^3)$. This equation is valid only when the distribution $P(\Omega, \Omega^\dagger, R^-, R^+, R^3)$ vanishes sufficiently rapidly at the boundaries. In practical applications, it is usually the case that the damping terms provide a strong bound at infinity on the distribution function [24].

In terms of these variables, and in the limit of large N, we get the following set of stochastic equations which serve as the basis for the simulation,

$$\begin{aligned}\left(\frac{\partial}{\partial z} + \frac{1}{c}\frac{\partial}{\partial t}\right)\Omega(t,z) &= -\frac{1}{2}\kappa\Omega(t,z) + \frac{G}{c}\int \rho(\mathbf{r},\omega)R^-(t,\mathbf{r},\omega)\,d\mathbf{r}_\perp d\omega + F^\Omega(t,z),\\ \frac{\partial}{\partial t}R^-(t,\mathbf{r},\omega) &= -[\gamma_\perp + i(\omega-\omega_0)]R^-(t,\mathbf{r},\omega) + u(\mathbf{r}_\perp)\Omega(t,z)R^3(t,\mathbf{r},\omega) + F^R(t,\mathbf{r},\omega),\\ \frac{\partial}{\partial t}R^3(t,\mathbf{r},\omega) &= -\gamma_\parallel[R^3(t,\mathbf{r},\omega) - \sigma^{SS}] - \frac{1}{2}[u(\mathbf{r}_\perp)\Omega(t,z)R^+(t,\mathrm{r},\omega) + u^*(\mathbf{r}_\perp)\Omega^\dagger(t,z)R^-(t,\mathbf{r},\omega)] + F^z(t,\mathbf{r},\omega),\end{aligned} \tag{2.18}$$

where

$$\sigma^{SS} = \frac{W_{12} - W_{21}}{W_{12} + W_{21}}. \tag{2.19}$$

Equations (2.18) are identical with the usual semiclassical equations for the slowly varying envelope fields [25,26], except for the presence of the Langevin terms F that describe quantum fluctuations and depend on the bath and nonlinear atom-field coupling, and are expressed as

$$F^\Omega(t,z) = 2\xi^\alpha(t,z)\sqrt{\frac{G\kappa\overline{n}}{c}} = [F^{\Omega^\dagger}(t,z)]^*,$$

$$F^R(t,\mathbf{r},\omega) = \frac{1}{\sqrt{\rho(\mathbf{r},\omega)}}\{\xi^J(t,\mathbf{r},\omega)\sqrt{2u(\mathbf{r}_\perp)\Omega R^-} + 2\xi^P(t,\mathbf{r},\omega)\sqrt{\gamma_P(R^3+1)} + 2\xi^o(t,\mathbf{r},\omega)\sqrt{W_{12}}\},$$

$$F^{R^\dagger}(t,\mathbf{r},\omega)=\frac{1}{\sqrt{\rho(\mathbf{r},\omega)}}\{\xi^{J^\dagger}(t,\mathbf{r},\omega)\sqrt{u^*(\mathbf{r}_\perp)\Omega^\dagger R^+}+2\xi^{P*}(t,\mathbf{r},\omega)\sqrt{\gamma_P(R^3+1)}+2\xi^{o*}(t,\mathbf{r},\omega)\sqrt{W_{12}}\},$$
$$F^z(t,\mathbf{r},\omega)=\frac{1}{\sqrt{\rho(\mathbf{r},\omega)}}\{\xi^z(t,\mathbf{r},\omega)\sqrt{[2\gamma_\parallel(1-\sigma^{SS}R^3)}+[R^-u^*(\mathbf{r}_\perp)\Omega^\dagger-R^+u(\mathbf{r}_\perp)\Omega-2W_{12}R^+R^-]^{1/2}$$
$$-[\xi^o(t,\mathbf{r},\omega)R^+ +\xi^{o*}(t,\mathbf{r},\omega)R^-]\sqrt{W_{12}}\}. \tag{2.20}$$

The terms optical thermal noise $\xi^\alpha(t,z)$, incoherent pumping noise $\xi^o(t,\mathbf{r},\omega)$, and collisional dephasing noise $\xi^P(t,\mathbf{r},\omega)$ are complex, while the photon-atom interaction noises $\xi^J(t,\mathbf{r},\omega)$, $\xi^{J^\dagger}(t,\mathbf{r},\omega)$, $\xi^z(t,\mathbf{r},\omega)$ are real. The correlation properties are

$$\begin{aligned}
&\langle\xi^\alpha(t,z)\xi^{\alpha*}(t',z')\rangle=\delta(t-t')\delta(z-z'),\\
&\langle\xi^o(t,\mathbf{r},\omega)\xi^{o*}(t',\mathbf{r}',\omega')\rangle=\delta(t-t')\delta^{(3)}(\mathbf{r}-\mathbf{r}')\delta(\omega-\omega'),\\
&\langle\xi^P(t,\mathbf{r},\omega)\xi^{P*}(t',\mathbf{r}',\omega')\rangle=\delta(t-t')\delta^{(3)}(\mathbf{r}-\mathbf{r}')\delta(\omega-\omega'),\\
&\langle\xi^J(t,\mathbf{r},\omega)\xi^J(t',\mathbf{r}',\omega')\rangle=\delta(t-t')\delta^{(3)}(\mathbf{r}-\mathbf{r}')\delta(\omega-\omega'),\\
&\langle\xi^{J^\dagger}(t,\mathbf{r},\omega)\xi^{J^\dagger}(t',\mathbf{r}',\omega')\rangle=\delta(t-t')\delta^{(3)}(\mathbf{r}-\mathbf{r}')\delta(\omega-\omega'),\\
&\langle\xi^z(t,\mathbf{r},\omega)\xi^z(t',\mathbf{r}',\omega')\rangle=\delta(t-t')\delta^{(3)}(\mathbf{r}-\mathbf{r}')\delta(\omega-\omega').
\end{aligned} \tag{2.21}$$

Since the equations are derived through a normally ordered representation, there are bath noise terms associated with dephasing (γ_p) and gain (W_{12}), but not loss (W_{12}). Furthermore, the gain noise is only present at finite temperatures. In addition to the bath noise, the positive P method has noise associated with the atom-field coupling, which is present even for unitary evolution and corresponds in some sense to shot-noise effects in the atom-light interaction. In addition, c represents the speed of light in the fiber, taking into account linear dispersion.

III. RESULTS

A. Amplitude squeezing

For the purpose of illustrating the method, we make the additional simplification that the transverse mode is uniform. The atomic fields can then also be considered as a function of z only. To solve the system (2.18) it proves convenient to use a propagating reference frame moving with the center of the pulse in the propagation direction z with the velocity v_g, and thus involving a retarded time [27,28] $\tau=t-z/v_g$. In this retarded frame, the first equation in (2.18) becomes

$$\left[\frac{\partial}{\partial z}+\left(\frac{1}{c}-\frac{1}{v_g}\right)\frac{\partial}{\partial\tau}\right]\Omega(\tau,z)$$
$$=-\frac{1}{2}\kappa\Omega(\tau,z)+\frac{G}{c}\int\rho(z,\omega)R^-(\tau,z,\omega)d\omega+F^\Omega(\tau,z). \tag{3.1}$$

For a coherent field the appropriate initial condition is

$$P(\tau,\Omega,\Omega^\dagger)=\delta^{(2)}(\Omega^*-\Omega^\dagger)\delta^{(2)}[\Omega-\mathcal{E}(0,\tau)], \tag{3.2}$$

with $\mathcal{E}(z,\tau)$ being the soliton-shaped pulse in the retarded time frame,

$$\mathcal{E}(z,\tau)=2A\cosh^{-1}[A(\tau-\tau_0)]\exp\{i[\delta\tau+\phi(z)]\},$$
$$\phi(z)=\frac{\delta}{A^2+\delta^2}G\rho z/c, \tag{3.3}$$

where $2A$ is the pulse amplitude, τ the pulse timing, δ is detuning, $\phi(z)$ is the phase, and v_g obeys

$$\frac{1}{v_g}=\frac{1}{c}+\frac{1}{2}\frac{G\rho/c}{A^2+\delta^2}. \tag{3.4}$$

For the atoms initially distributed in the ground state we have the initial condition

$$R^+=R^-=0,\quad R^3=-\frac{1}{2}. \tag{3.5}$$

We next concentrate on amplitude squeezing, which is more easily detectable. Therefore, we want to analyze the fluctuations of the integrated pulse intensity:

$$\hat{M}(z)\equiv\int dt\hat{\Omega}^\dagger(t,z)\hat{\Omega}(t,z). \tag{3.6}$$

We work with elapsed time where the pulse envelope can be assumed to be stationary (i.e., the transit time of the pulse). Then the equal-space commutation relations of the field operators (in the interaction picture) are

$$[\hat{\Omega}(t,z),\hat{\Omega}^\dagger(t',z)]=4g^2\sum_{m,m'}[e^{-i\omega_m t}\hat{a}_m,e^{i\omega_{m'}t'}\hat{a}^\dagger_{m'}]$$
$$=4g^2\sum_m e^{-i\omega_m(t-t')}, \tag{3.7}$$

which in the continuum limit becomes

$$[\hat{\Omega}(t,z),\hat{\Omega}^\dagger(t',z)]=\frac{4g^2}{\Delta\omega}\int d\omega e^{-i\omega(t-t')}=\frac{4G}{v_g}\delta(t'-t), \tag{3.8}$$

where we have made use of $\Delta\omega\simeq(d\omega/dk)\Delta k=2\pi v_g/L$, with group velocity v_g.

Using this relation, we can write the variance of $\hat{M}$ in terms of normally ordered quantities. If we notice that

$$\hat{M}^2=\int dtdt'\hat{\Omega}^\dagger(t,z)\hat{\Omega}(t,z)\hat{\Omega}^\dagger(t',z)\hat{\Omega}(t',z)$$
$$=:\hat{M}^2:+\frac{4G}{v_g}\hat{M}, \tag{3.9}$$

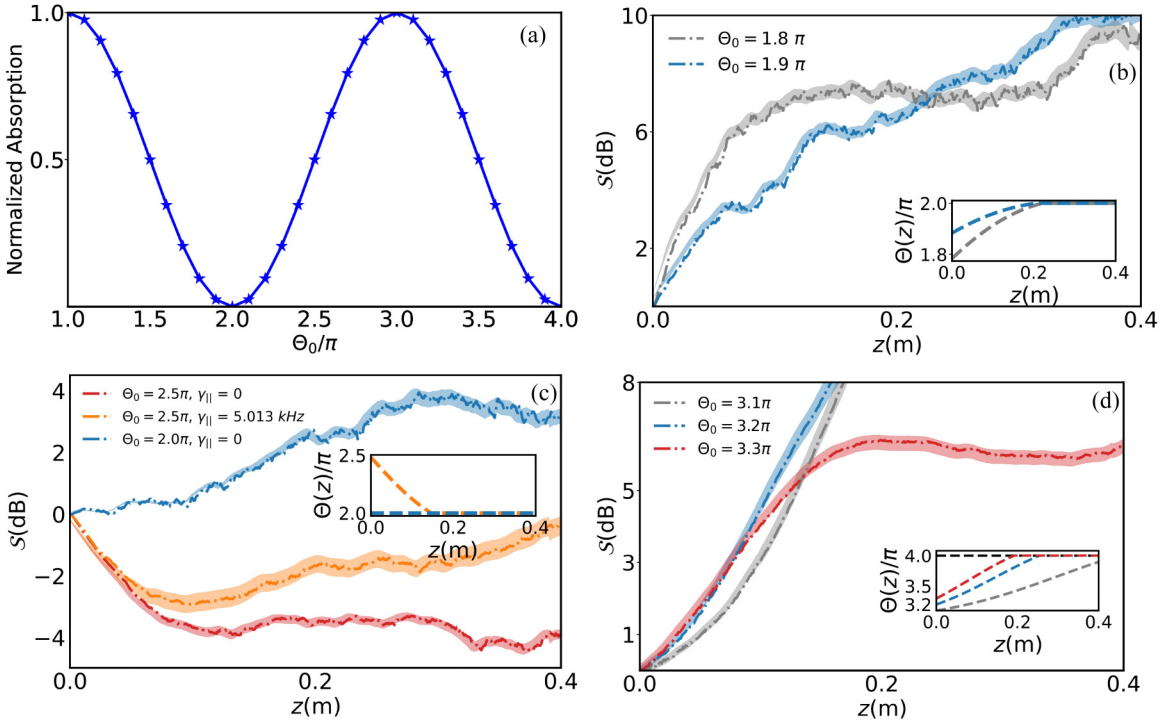

FIG. 2. (a) The normalized absorption of atoms (blue solid line) vs area. When Θ_0 takes values of π and 3π, the pulse leaves the atoms in the excited state. However, at $\Theta_0 = 2\pi$ and $\Theta_0 = 4\pi$, the pulse returns back the atoms to the ground state. Looking between the range of $\Theta_0 = \pi$ and $\Theta_0 = 2\pi$, or similarly 3π to 4π, atoms are left excited in some extent and the pulse area intensifies toward 2π (or 4π in the latter range) during the propagation. When the initial area ranges from 2π to 3π, atoms are left again excited but the pulse area shrinks toward 2π during the propagation. (b) Excess noise as a function of the fiber length for $\Theta_0 = 1.8\pi, 1.9\pi$ (the inset subplot indicates the growth of the pulse area during propagation along the fiber). (c) Comparison of the squeezing of two input pulses with initial area 2π and 2.5π during their propagation into the fiber. In the case of $\Theta_0 = 2.5\pi$, the amplitude squeezing is plotted in the presence and the absence of damping. The shaded area around the dashed blue, red, and orange line indicates the uncertainty of the amplitude squeezing in each grid point. (d) Squeezing for pulses with $\Theta_0 = 3.1\pi, 3.2\pi, 3.3\pi$ (the subplot shows the pulse area propagation within the fiber before and after it reaches to the stable area $\Theta = 4\pi$). We have set the optical pulse duration for $3\pi < \Theta_0 < 2\pi$ to be $\tau = 9.7$ ns and for $2\pi < \Theta_0 < 3\pi$ to be 99.97 ns. The atom-field coupling $G = 0.001\,742\,4\ \mathrm{s}^{-2}$ m and the atomic wavelength $\lambda_0 = 9956.1$ Å are considered. The optical pulse is on resonance, and the atoms have a homogeneously broadening line shape at zero temperature. The total atom number in the fiber is 10^8, and the linear optical losses $\kappa = 0$.

where : : indicates normal ordering, the variance can thus be written

$$\mathrm{Var}(\hat{M}) = \mathrm{Var}_P(\hat{M}) + \frac{4G}{v_g}\langle\hat{M}\rangle. \tag{3.10}$$

Here, $\mathrm{Var}_P(\hat{M}) \equiv \langle{:}\hat{M}^2{:}\rangle - \langle\hat{M}\rangle^2$ is the normally ordered variance that can be calculated directly from the positive P variables.

Note that for a coherent state $\langle{:}\hat{M}^2{:}\rangle = \langle\hat{M}\rangle^2$ and thus

$$\mathrm{Var}_{\mathrm{coh}}(\hat{M}) = \frac{4G}{v_g}\langle\hat{M}\rangle. \tag{3.11}$$

Defining, as is usual, the squeezing with respect to the coherent-state level, we obtain the squeezing ratio

$$S \equiv \frac{\mathrm{Var}(\hat{M})}{\mathrm{Var}_{\mathrm{coh}}(\hat{M})} = 1 + \frac{v_g}{4G}\frac{\mathrm{Var}_P(\hat{M})}{\langle\hat{M}\rangle}. \tag{3.12}$$

The area of a pulse is defined as [29]

$$\Theta(z) = \int \Omega(\tau, z)d\tau. \tag{3.13}$$

For a hyperbolic secant soliton $\Theta_0 = 2\pi$, the pulse shape remains unchanged during propagation. However, any initial pulse area Θ_0 that satisfies $(m+1)\pi > m\pi\,\Theta_0$ will grow in area towards $(m+1)\pi$ if m is an odd number or it will shrink in area towards $m\pi$ if m is an even number. Figure 2(a) shows the total absorbed energy by atoms as a function of area.

Since when $\Theta_0 = 2\pi$ the pulse amplitude remains unchanged, there is no reduction in the fluctuations of the soliton amplitude. Consequently, no amplitude squeezing occurs. For pulses $\pi < \Theta_0 < 2\pi$, the area will grow until it reaches the stable value $\Theta_0 = 2\pi$. This leads to an increase in the amplitude fluctuations leading to no amplitude squeezing, as can be appreciated in Fig. 2(b).

However, if we consider a pulse with $\Theta_0 = 2.5\pi$, the pulse area is not stable during the propagation and it diminishes towards $\Theta = 2\pi$. As a result, the pulse loses energy and leaves the atoms excited. Our simulation shows that this reduction in the pulse area results in diminished amplitude fluctuations, ultimately leading to amplitude squeezing.

Figure 2(c) displays the calculated amplitude squeezing as a function of fiber length for two different initial pulse areas. The results reveal a precisely 2π soliton pulse exhibits no amplitude squeezing during the pulse propagation along the fiber, whereas a pulse with an initial area of 2.5π undergoes squeezing after propagating a distance of $z = 0.4$ m,

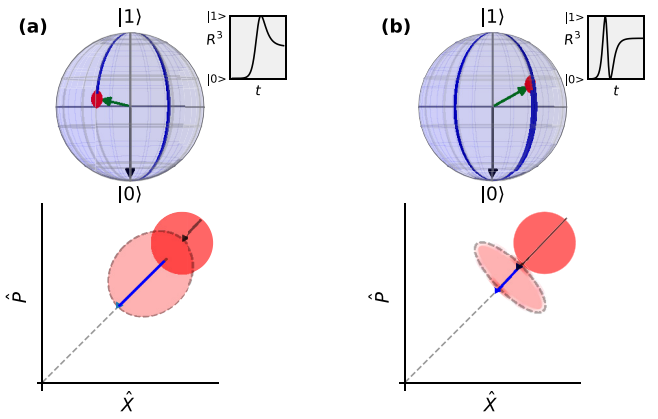

FIG. 3. At the top, we show the atomic evolution as both a trajectory of the Bloch vector and as the time evolution of the population inversion (gray inset). At the bottom the phase-space representation of the excitation of the pulse is shown: the coherent state before the interaction (red) and the distorted state after the interaction (pink). In (a) the initial pulse area is less than 2π and in (b) the pulse area is larger than 2π. The atomic excitation left behind corresponds to an attenuation of the light pulse. In (a) larger amplitudes within the uncertainty region are attenuated less than lower amplitudes resulting in increased amplitude uncertainty. In (b) the roles are reversed: Larger amplitudes are attenuated more than lower ones, leading to squeezing of the amplitude uncertainty.

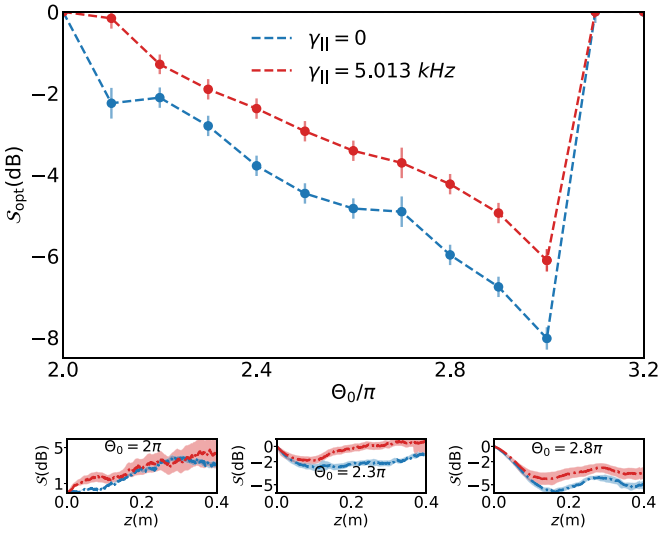

FIG. 4. Optimum squeezing as a function of the initial area of the input pulse in the presence and absence of longitudinal damping. The bottom subplots indicate the evolution of squeezing for pulses with the initial area 2π, 2.3π, and 2.8π. The blue curves are in the absence of the longitudinal damping while the red curves capture the effect of the damping. The transparent shaded color shows the uncertainty of the achieved squeezing from 4000 samples in each grid point. The longitudinal damping rate is taken to be $\gamma_{\|} = 5.013$ kHz, while temperature is kept at zero. The pulse duration $\tau = 99.97$ ns and the atomic properties are the same as in Fig. 2.

but before reaching the stable area 2π. The simulation reveals amplitude squeezing of approximately -4 dB in this case.

In contrast, when the initial area is considered $\Theta_0 > 3\pi$, the pulse area intensifies until it reaches 4π. Hence the pulse amplitude fluctuations increase, and no squeezing is observed; see Fig. 2(d). An intuitive picture of these facts can be seen in Fig. 3.

We can think of the results as a consequence of the pulse reshaping area. When the pulse area shrinks toward $m\pi$, where m is an even number, the fluctuations get squeezed. On the other hand, when the pulse expands towards $m\pi$, the fluctuations are antisqueezed.

B. Optimal squeezing

We next examine the effect of the longitudinal damping $\gamma_{\|}$ on the amplitude squeezing. Specifically, we compare the results when the longitudinal damping is treated as $\gamma_{\|} = \gamma_0$ with the previous scenario where longitudinal damping was assumed to be zero.

Figure 4 illustrates the optimal squeezing as a function of the pulse area, both in the presence and absence of longitudinal damping. The error bar on each data point is calculated from 4000 samples. It is evident that taking into account $\gamma_{\|}$ leads to a decrease in the amplitude squeezing. Longitudinal damping enhances the decay of atoms into the ground state and this continuous decay process disrupts the Rabi frequency and contributes to increased amplitude pulse fluctuations, resulting in the reduction of amplitude squeezing observed in the system. Since the temperature is taken as zero in Fig. 3, there is no contribution of thermal noise. The remaining sources of noise originate from the dipole-field interaction and spontaneous emission.

Looking at Fig. 2(a), the pulse energy loss has its maximum at $\Theta_0 = 3\pi$, the incident pulse with $\Theta_0 = 3\pi$ undergoes the greatest reshaping before it reaches to the stable area, $\Theta_0 = 2\pi$. Consequently, starting with a pulse with $\Theta_0 = 3\pi$ results in the most pronounced reduction of amplitude fluctuations, and eventually leading to the squeezing dip.

Furthermore, the effect of damping on the optimum squeezing for each pulse is shown in the subplots in Fig. 3. The three subplots indicate the squeezing in the presence and absence of longitudinal damping within the fiber for $\Theta_0 = 2\pi$, $\Theta_0 = 2.3\pi$, and $\Theta_0 = 2.8\pi$. Comparing the two pulses with $\Theta_0 = 2.3\pi$ and the other with an area of 2.8π, the pulse with 2.3π reaches the stable area sooner. As a result, the optimum squeezing ($\mathcal{S}_{\text{opt}}$) occurs over a shorter distance for the 2.3π pulse, as illustrated in Fig. 4.

It is interesting to check the minimum length required for a pulse to reach its soliton power. This is shown in Fig. 5 for a pulse of duration $\tau = 99.77$ ns. We can appreciate that this length is fairly independent of the longitudinal damping and increases quadratically with the initial pulse area Θ_0.

Figure 6 illustrates the effect of detuning on amplitude squeezing. The simulation concludes that the small detunings have little effect on the squeezing. Only for large detuning do we observe a significant decrease in squeezing.

In Fig. 7, the impact of temperature on the squeezing is examined, for the particular case of a pulse with $\Theta_0 = 2.8$. All sources of noise, including thermal noise and spontaneous emission, are taken into account. In addition, atoms

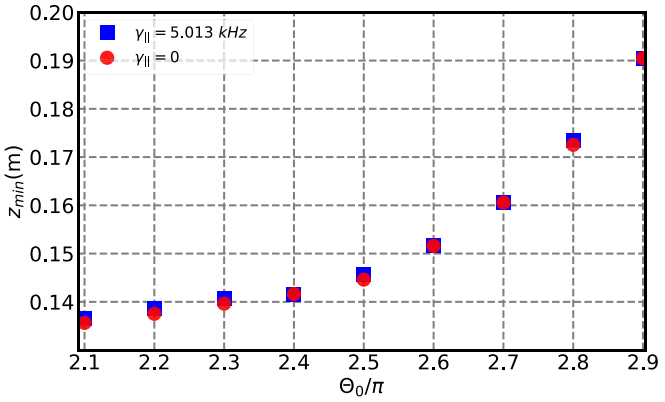

FIG. 5. Minimum length required for the pulse to reach a soliton power, as a function of the initial area. The pulse duration is $\tau = 99.73$ ns and the atomic properties are the same as those presented in Fig. 2.

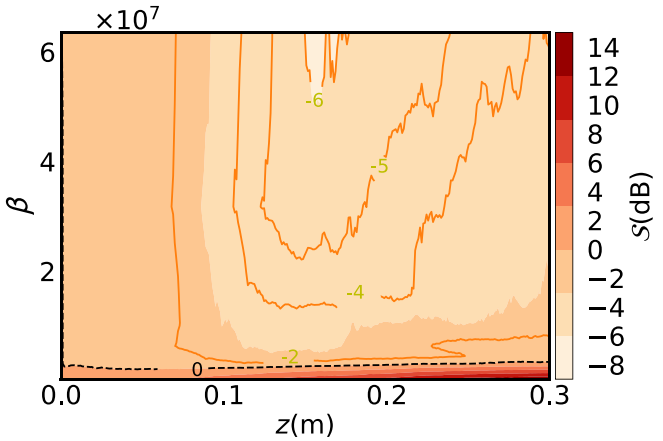

FIG. 7. Density plot of the squeezing as a function of the temperature (in units of β) and the distance for an optical resonant pulse with $\tau = 99.97$ ns and initial area $\Theta_0 = 2.8$. The atoms are detuned by $\Delta\omega_{\text{Doppler}}$ with an inhomogeneously broadening line shape. The atomic wavelength $\lambda_0 = 9956.1$ Å, the atom-field strength is $G = 0.001\,742\,4\ \text{s}^{-2}\,\text{m}$, and due to the short fiber length and short pulse duration, we assume the linear optical losses to be $\kappa = 0$. The squeezing is calculated over 2000 samples in this data set.

experience a Doppler broadening as the temperature increases. In terms of $\beta = \hbar\omega_0/k_B T$, where $\omega_0 = 8.218\,84 \times 10^{14}$ Hz, the highest squeezing occurs within the range $\beta = 2$–6×10^7, which corresponds to temperatures in the range of microdegrees Kelvin. Note that the data set is not optimized: Depending on the system parameters, such as the number of atoms and pulse characteristics, one might achieve different optimal regimes for the amplitude squeezing.

The effect of a small spontaneous emission rate on the amplitude squeezing exhibits a resemblance to the impact of damping. Figure 8 illustrates the optimal squeezing achieved for various strengths of γ_0. In the weak γ_0 regime, a squeezing level of -4 dB is attained. The inset in Fig. 8 illustrates how squeezing evolves concerning γ_0 along the fiber. Within the weak γ_0 strength regime, the highest amplitude squeezing occurs towards the fiber's end. There are two primary reasons for this. First, weak γ_0 results in a smaller coupling strength, causing the pulse to move more slowly through the medium. Second, this condition also reduces the medium's noise level. However, in the moderate regimes, the squeezing significantly diminishes.

IV. CONCLUDING REMARKS

Resorting to the formalism of the positive P function, we have developed a full quantum model of SIT that has allowed us to characterize the dynamic behavior of amplitude squeezing. Our investigation encompassed both the influence of the thermal and quantum noise. Our results demonstrate a strong dependence of amplitude squeezing in SIT solitons on both the initial pulse area and the absorbed energy. Furthermore, we have shown that damping can noticeably diminish squeezing, even when temperature effects are negligible. However

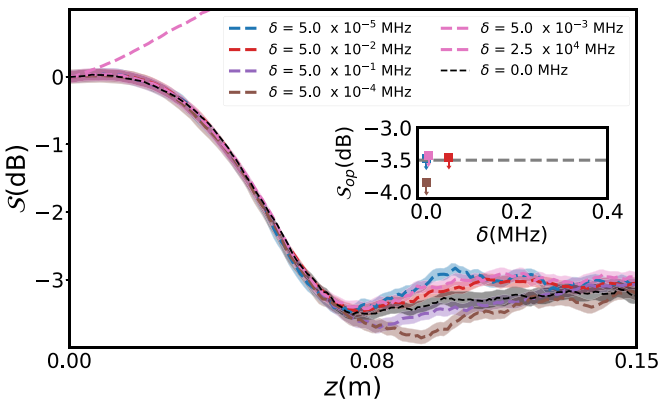

FIG. 6. Amplitude squeezing for detuned optical pulses length as a function of the distance z. The subplot gives the optimum value of squeezing for each one of the detunings marked in the inset. The pulse duration is $\tau = 0.002$ ns with the initial area $\Theta_0 = 2$, the atomic wavelength $\lambda_0 = 3650.15$ Å, the spontaneous emission rate $\gamma_0 = 0.0889$ GHz, and the linear optical losses $\kappa = 0$.

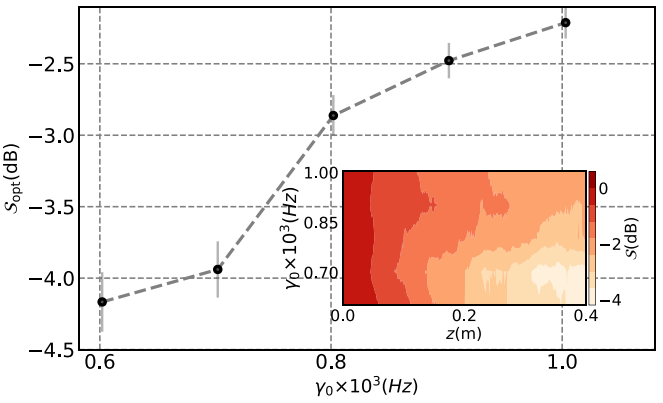

FIG. 8. The impact of spontaneous emission rate γ_0 on the amplitude squeezing is shown. The plot displays the optimum value of the amplitude squeezing (S_{opt}) achieved from 2000 samples for a range of γ_0 between 0.6 to 1.0 kHz. The subplot indicates the evolution of squeezing within the fiber for each γ_0. The initial area of the input pulse is set to be 2.3π. The thermal noise is kept zero.

the primary detrimental impact arises from the thermal noise, leading to a complete suppression of squeezing.

Due to the potential of SIT for generating pulse-squeezed states, it has found applications in numerous areas of quantum optics, such as quantum nondemolition measurements [30] or information storage [31]. Optical cooperative phenomena, such as SIT, exhibit specific features that provide the ground for addressing fundamental problems in modern quantum information. The progress in ultrashort pulse measurements [32–34] makes SIT a good candidate for the development of high-precision photonic technologies [35].

Nonetheless, gas-filled hollow-core fibers also present challenges and potential drawbacks. The process of filling the fiber with a suitable gas is notably complex. One specific concern involves alkali vapors, which have a not well understood tendency to bind with and diffuse into the glass. This makes it challenging to load the fibers and to maintain a permanent high vapor pressure inside the core. However, the Joly group [36] has reported successful mitigation of this issue in their work. Moreover, as is true for all relatively pure quantum states, the performance of systems in such states is susceptible to environmental influences, with temperature fluctuations and vibrations posing significant threats. External perturbations have the potential to disrupt the stability and coherence of the squeezed light. This introduces some complexities in maintaining the desired quantum properties.

The technological usage of single-mode or two-mode squeezed (entangled) quantum properties of light to enhance the performance of optical systems, depends on the details of parameters such as degree of squeezing, optical bandwidth, noise bandwidth, and the wavelength range. The details of the generation process are immaterial for that purpose. Therefore, it is important to study the various squeezed-state generation schemes in order to understand which parameter is best achieved with which generation scheme. Squeezing by SIT is one that is relevant for these generation schemes.

In summary, experimentally observing squeezing effects in self-induced transparency (SIT) solitons is feasible, particularly by utilizing ultrashort pulses with durations shorter than the characteristic timescales of the involved atoms. Mercury atoms, previously employed within hollow-core fibers [14], are a viable candidate due to their resonant properties. However, the short wavelength of mercury necessitates the use of ultrashort pulses for efficient excitation. Alternatively, alkali atoms possess longer wavelengths than mercury, making them attractive candidates if one overcomes the mentioned challenges. In future studies, we aim to investigate the essential conditions utilizing alkali atoms and mercury atoms.

ACKNOWLEDGMENTS

We are indebted to R. K. Lee and T. Dirmeier for discussions. L.L.S.-S. acknowledges financial support from Spanish Agencia Estatal de Investigación (Grant No. PID2021-127781NB-I00). A.A.S. acknowledges financial support from the Ministry of Science and Higher Education of the Russian Federation (Grant No. 075-15-2022-316) and from the Foundation for the Advancement of Theoretical Physics and Mathematics "BASIS." G.L. acknowledges financial support from German BMBF (Grant No. VDI-Tz 13N15329).

[1] G. L. Lamb, Analytical descriptions of ultrashort optical pulse propagation in a resonant medium, Rev. Mod. Phys. **43**, 99 (1971).

[2] R. E. Slusher, Self-induced transparency, Prog. Opt. **12**, 53 (1974).

[3] I. A. Poluéktov, Y. M. Popov, and V. S. Roĭtberg, Self-induced transparency effect, Sov. Phys. Usp. **17**, 673 (1975).

[4] A. I. Maimistov, A. M. Basharov, S. O. Elyutin, and Y. M. Sklyarov, Present state of self-induced transparency theory, Phys. Rep. **191**, 1 (1990).

[5] S. L. McCall and E. L. Hahn, Self-induced transparency by pulsed coherent light, Phys. Rev. Lett. **18**, 908 (1967).

[6] S. L. McCall and E. L. Hahn, Self-induced transparency, Phys. Rev. **183**, 457 (1969).

[7] L. Allen and J. H. Eberly, *Optical Resonance and Two-Level Atoms* (Dover, New York, 1975).

[8] L. Mandel and E. Wolf, *Optical Coherence and Quantum Optics* (Cambridge University, Cambridge, UK, 1995).

[9] M. O. Scully and S. Zubairy, *Quantum Optics* (Cambridge University Press, Cambridge, UK, 1997).

[10] K. Watanabe, H. Nakano, A. Honold, and Y. Yamamoto, Optical nonlinearities of excitonic self-induced-transparency solitons: Toward ultimate realization of squeezed states and quantum nondemolition measurement, Phys. Rev. Lett. **62**, 2257 (1989).

[11] P. D. Drummond, R. M. Shelby, S. R. Friberg, and Y. Yamamoto, Quantum solitons in optical fibres, Nature (London) **365**, 307 (1993).

[12] R. Bullough and H. Gibbs, Information storage and retrieval by stopping pulses of light, J. Mod. Opt. **51**, 255 (2004).

[13] P. S. J. Russell, Photonic-crystal fibers, J. Lightwave Technol. **24**, 4729 (2006).

[14] U. Vogl, F. Sedlmeir, N. Joly, C. Marquardt, and G. Leuchs, Generation of non-classical light via self-induced transparency in mercury-filled hollow core photonic crystal fibers, in *Frontiers in Optics 2016, OSA Technical Digest (online)* (Optica Publishing Group, Washington, DC, 2016), paper FW5F-4.

[15] Y. Lai and H. A. Haus, Quantum theory of self-induced transparency solitons: A linearization approach, Phys. Rev. A **42**, 2925 (1990).

[16] A. Shabat and V. Zakharov, Exact theory of two-dimensional self-focusing and one-dimensional self-modulation of waves in nonlinear media, Sov. Phys. JETP **34**, 62 (1972).

[17] R.-K. Lee and Y. Lai, Quantum squeezing and correlation of self-induced transparency solitons, Phys. Rev. A **80**, 033839 (2009).

[18] Y. Lai and S.-S. Yu, General quantum theory of nonlinear optical-pulse propagation, Phys. Rev. A **51**, 817 (1995).

[19] P. D. Drummond and M. G. Raymer, Quantum theory of propagation of nonclassical radiation in a near-resonant medium, Phys. Rev. A **44**, 2072 (1991).

[20] P. D. Drummond and C. W. Gardiner, Generalised *P*-representations in quantum optics, J. Phys. A: Math. Gen. **13**, 2353 (1980).

[21] C. W. Gardiner and P. Zoller, *Quantum Noise*, 2nd ed. (Springer, Berlin, 2004).

[22] M. Hollas, *Modern Spectroscopy*, 3rd ed. (Wiley, New York, 1996).

[23] H.-P. Breuer and F. Petruccione, *The Theory of Open Quantum Systems* (Oxford University Press, Oxford, UK, 2002).

[24] A. Gilchrist, C. W. Gardiner, and P. D. Drummond, Positive *P* representation: Application and validity, Phys. Rev. A **55**, 3014 (1997).

[25] M. Lax, Quantum noise. IV. Quantum theory of noise sources, Phys. Rev. **145**, 110 (1966).

[26] H. Haken and W. Weidlich, Quantum noise operators for the *N*-level system, Z. Phys. **189**, 1 (1966).

[27] V. V. Kozlov and A. B. Matsko, Stochastic theory of self-induced transparency: Linearized approach, J. Opt. Soc. Am. B **17**, 1031 (2000).

[28] J. F. Corney, J. Heersink, R. Dong, V. Josse, P. D. Drummond, G. Leuchs, and U. L. Andersen, Simulations and experiments on polarization squeezing in optical fiber, Phys. Rev. A **78**, 023831 (2008).

[29] H. A. Haus, K. Watanabe, and Y. Yamamoto, Quantum-nondemolition measurement of optical solitons, J. Opt. Soc. Am. B **6**, 1138 (1989).

[30] A. B. Matsko, V. V. Kozlov, and M. O. Scully, Backaction cancellation in quantum nondemolition measurement of optical solitons, Phys. Rev. Lett. **82**, 3244 (1999).

[31] M. Bajcsy, A. S. Zibrov, and M. D. Lukin, Stationary pulses of light in an atomic medium, Nature (London) **426**, 638 (2003).

[32] F. Krausz and M. Ivanov, Attosecond physics, Rev. Mod. Phys. **81**, 163 (2009).

[33] U. Keller, Ultrafast solid-state laser oscillators: A success story for the last 20 years with no end in sight, Appl. Phys. B **100**, 15 (2010).

[34] R. M. Arkhipov, M. V. Arkhipov, A. A. Shimko, A. V. Pakhomov, and N. N. Rosanov, Ultrashort optical pulses and their generation in resonant media, JETP Lett. **110**, 15 (2019).

[35] C. Jirauschek, M. Riesch, and P. Tzenov, Optoelectronic device simulations based on macroscopic Maxwell–Bloch equations, Adv. Theory Simul. **2**, 1900018 (2019).

[36] D. Häupl, D. Weller, R. Löw, and N. Joly, Spatially resolved spectroscopy of alkali metal vapour diffusing inside hollow-core photonic crystal fibres, New J. Phys. **24**, 113017 (2022).